# A Potassium Channel β Subunit Couples Mitochondrial Electron Transport to Sleep

**Anissa Kempf**[#1], **Seoho M. Song**[#1], **Clifford B. Talbot**[1], and **Gero Miesenböck**[1]

[1]Centre for Neural Circuits and Behaviour, University of Oxford, Tinsley Building, Mansfield Road, Oxford, OX1 3SR, United Kingdom

[#] These authors contributed equally to this work.

## Abstract

The essential but enigmatic functions of sleep[1,2] must be reflected in molecular changes sensed by the brain's sleep-control systems. In *Drosophila*, two dozen sleep-inducing neurons[3] with projections to the dorsal fan-shaped body (dFB) adjust their electrical output to sleep need[4], via the antagonistic regulation of two potassium conductances: the leak channel Sandman imposes silence during waking, whereas augmented A-type currents through Shaker support tonic firing during sleep[5]. Here, we report that oxidative by-products of mitochondrial electron transport[6,7] regulate the activity of dFB neurons through a nicotinamide adenine dinucleotide phosphate (NADPH) cofactor bound to the oxidoreductase domain[8,9] of Shaker's $K_V\beta$ subunit, Hyperkinetic[10,11]. Sleep loss elevates mitochondrial reactive oxygen species in dFB neurons, which register this rise by converting Hyperkinetic to the $NADP^+$-bound form. The oxidation of the cofactor slows the inactivation of the A-type current and boosts the frequency of action potentials, thereby promoting sleep. Energy metabolism, oxidative stress, and sleep, three processes implicated independently in lifespan, aging, and degenerative disease[6,12–14], are thus mechanistically connected. $K_V\beta$ substrates[8,15,16] or inhibitors capable of altering the $NADP^+$:NADPH ratio (and hence the neurons' record of sleep debt or waking time) define novel prototypes of sleep-regulatory drugs.

Like sleep-active cells of the mammalian hypothalamus[17], dFB neurons in sleeping flies tend to be electrically active. To cause awakening, dopamine, acting directly on these cells[5], attenuates the voltage-gated A-type current[18] ($I_A$) carried by Shaker and upregulates a voltage-independent leak current through the two-pore domain channel Sandman[5]. Sandman

translocates from an intracellular storage pool to the plasma membrane, where it opens a potassium shunt that short-circuits the spike generator and switches the sleep-inducing neurons OFF5. The reverse switch, of dFB neurons to their electrically active state, is at the core of the organism's response to sleep loss4. We are therefore able to frame the question of sleep's biological role as a mechanistically well-defined problem: which signals or processes switch dFB neurons ON? Knowing the leading parts played in the excitability switch by Shaker and Sandman focuses the search for answers on two molecular events: the modulation of the Shaker current, and the internalization of Sandman. Our spotlight here is on Shaker.

Shaker coassembles with a β subunit called Hyperkinetic10 into a voltage-gated potassium channel with fourfold rotational symmetry9. The N-terminal domains of four Shaker subunits form a hanging platform, suspended below the voltage sensors of the channel, to which a Hyperkinetic tetramer docks. Hyperkinetic and other $K_V\beta$ subunits are related in sequence10,19 and structure8,9 to aldo-keto-reductases, complete with a catalytic tyrosinate anion, charge-relay system, and NADPH cofactor in their active sites. Oxidation or reduction of the stably bound nicotinamide by small-molecule substrates8,15,16 can alter the voltage-dependent activation and/or inactivation kinetics of the channels10,15,20. The functional purpose of coupling a cell's excitability to its metabolism, however, remains mysterious8,9.

Mutations in Shaker or Hyperkinetic both cause insomnia11,13. Unsurprisingly, given the importance of $I_A$ for sustaining the sleep-promoting activity of these cells5, dFB neurons are a major sleep-relevant site of action for both channel subunits: the depletion of either gene product from these cells alone, using *R23E10-GAL4*-restricted4 RNA interference (RNAi), reproduces the sleep disruptions of the genomic mutations5. To complement these demonstrations of necessity with a test of sufficiency, we restored Hyperkinetic expression exclusively in the dFB of otherwise homozygous mutant flies. Sleep returned to wild-type levels, but only if Hyperkinetic's active site was intact (Fig. 1a, b): a putative rescue transgene encoding a variant21 with a point mutation (K289M) that abolishes the protein's oxidoreductase activity15,20 but leaves its expression15,20,21 and the amplitude of $I_A$ unaltered (see later) proved ineffective. This finding has three implications. First, it suggests that Hyperkinetic's sleep-regulatory role is tied to its ability to sense changes in cellular redox state, which are therefore expected to accompany changes in sleep pressure. Second, it predicts that perturbing the redox chemistry of dFB neurons will have consequences for sleep. And third, it identifies a biophysical mechanism for coupling redox chemistry and sleep. Because redox reactions, oxygen use, and ATP synthesis are linked at the level of the flow of reducing equivalents through the mitochondrial electron transport chain, dFB neurons may monitor redox processes as a gauge of energy metabolism.

To examine the first of these implications, we compared the redox histories of flies that had been mechanically sleep-deprived with those of rested controls (Fig. 1c, d). The metabolic machinery of the inner mitochondrial membrane is the principal cellular source of oxidants, especially under conditions of ample NADH supply, large proton-motive force, and low ATP demand, when electrons stall in the transport chain and transfer directly to oxygen6,7, producing superoxide ($O_2^-$) that is subsequently dismuted to $H_2O_2$ (Fig. 2a). Chief conduits for electron leakage7 are a fully reduced ubiquinone pool and the resulting tailback of

electrons onto complex I. Although some reactive oxygen species (ROS) generated in mitochondria could conceivably reach the active site of Hyperkinetic by diffusion, a more plausible scenario is that $O_2^-$ and $H_2O_2$ react locally and release a longer-lived carbonyl substrate8 whose reduction by Hyperkinetic then causes the oxidation of NADPH. Lipid peroxidation products, such as the aldehyde 4-oxo-2-nonenal, serve as established hydride acceptors in $K_V\beta$ subunits15,16 and may represent the ill-defined electron densities9 overlying their hydrophobic active sites.

For a cumulative estimate of ROS production, we labeled the mitochondria of dFB neurons with a matrix-targeted fluorescent protein (MitoTimer) whose green-emitting chromophore converts irreversibly to red when oxidized22. We then deprived age-matched flies of variable amounts of sleep and determined the fluorescence emission ratio by two-photon microscopy. Mitochondrial ROS production rose with the size of the imposed sleep deficit: a night of sleep deprivation red-shifted MitoTimer's fluorescence relative to rested controls, but applying the same sleep deprivation protocol during the day, when flies are mostly awake, or adding a day to a night of sleep disruption produced only insignificant effects (Fig. 1c, d). Because dFB neurons generate few energetically costly action potentials in the awake, fed state, when calories are plentiful but the Sandman detent blocks spiking5, the condition of a high ATP:ADP ratio known to favour mitochondrial $O_2^-$ production6,7 from an abundance of reducing substrates is likely to be met. Consistent with this idea, mushroom body Kenyon cells, which are electrically active during waking, showed little evidence of oxidant exposure even after 24 h of sleep deprivation (Fig. 1d). In addition, or instead, dFB neurons may have an unusually low capacity for degrading ROS, making them canaries in the mine for their detection.

Curiously, flies expressing MitoTimer in dFB neurons lost ~2 h of baseline sleep per day (Fig. 2b). As the oxidation of MitoTimer will consume ROS, we interpret this finding as tentative evidence of a causal connection between mitochondrial oxidative burden and sleep. To strengthen this connection, we quantified sleep after three further dFB-neuron-specific interventions: manipulation of mitochondrial electron transport; chronic interference with antioxidant enzymes; and acute optogenetic induction of singlet oxygen ($^1O_2$) formation.

We first installed an electron overflow pathway in the inner mitochondrial membrane of dFB neurons by expressing the alternative oxidase AOX of *Ciona intestinalis*23,24. Like complex III, AOX taps into the ubiquinone pool, but instead of transferring an electron each to two cytochrome *c* carriers, it reduces molecular oxygen to water in a single four-electron transfer reaction (Fig. 2a). Alternative respiration thus siphons off electrons that would otherwise spill from the ubiquinone pool and produce ROS when the cytochrome branch of the transport chain is saturated or the availability of ADP is low6,7,23. Introducing AOX into the mitochondria of dFB neurons, which normally lack a capacity for alternative respiration, decreased daily sleep by nearly 7 h (Fig. 2c): clamping mitochondrial ROS production eased the pressure to sleep.

In animals without bifurcated electron transport chains, superoxide dismutases (SODs) and catalase, which acts as a sink for SOD-generated $H_2O_2$ and thereby pulls the dismutation reaction forward, form the first line of anti-oxidant defenses6,12 (Fig. 2a). Shoring up these

defenses in dFB neurons reduced sleep (Fig. 2d, e), while breaching them with the help of a mutant enzyme (SOD1$^{A4V}$) whose peroxidase activity is enhanced[25,26] had the converse effect; it increased sleep (Fig. 2d) without inhibiting waking locomotion (Extended Data Fig. 1a) or arousability (Extended Data Fig. 1b). The crucial link between redox chemistry and sleep was the Shaker–Hyperkinetic complex: the RNAi-mediated depletion of either channel subunit from dFB neurons not only occluded the sleep-promoting effect of SOD1$^{A4V}$ but reduced sleep below wild-type levels (Fig. 2d). In contrast, interference with the expression of Shal, a $K_V$ channel without a sleep-regulatory function in dFB neurons[5], proved innocuous (Fig. 2d).

Analogous SOD1 manipulations in cryptochrome- or PDF-positive clock neurons or Kenyon cells (which all have demonstrated roles in sleep control[27]) or in olfactory projection neurons (for which no such role has been reported) failed to influence sleep (Extended Data Fig. 2a–d). dFB neurons thus appear unique, at least among this comparison group, in their ability to transduce oxidative stress into sleep.

As a third test of the redox control of sleep, we anchored miniSOG, an engineered flavoprotein[28] that photogenerates $^1O_2$, via a myristoyl group at the cytoplasmic face of the plasma membrane[29] (Fig. 3a). If the light-driven release of $^1O_2$ near Hyperkinetic causes the oxidation of bound NADPH, either directly or via local lipid peroxidation, it should be possible to bypass the chain of events that couples this final transduction step to mitochondrial respiration and induce sleep acutely. Indeed, during a 30-min observation interval that began with a 9-min exposure to blue light, flies expressing miniSOG in dFB neurons fell quiescent in greater proportion, and for longer, than control flies did (Fig. 3b, c). Epochs of quiescence outlasted the illumination period by ~1 h (Fig. 3d), could be blocked by the removal of Hyperkinetic but not of Shal (Fig. 3b, c), and were not due to the suppression of waking movements (Extended Data Fig. 1c) or a confounding influence of cryptochrome photoreceptors[21] (Extended Data Fig. 3).

Whole-cell recordings from dFB neurons, before and after miniSOG-mediated photooxidation under sleep-inducing conditions, revealed some of the well-documented biophysical changes underpinning the wake–sleep switch[4,5]: the neurons' action potential responses to depolarizing current became more vigorous (Fig. 4a–c); their membrane time constants lengthened (Fig. 4b); the interspike interval contracted (Fig. 4a, c); and fast $I_A$ inactivation slowed (Fig. 4d, e, Extended Data Table 1). Because A-type channels in the conducting state are the repolarizing force that returns the membrane potential to its resting level after a spike, changes in inactivation kinetics influence firing rates[18]. Both are regulated by $K_V\beta$ subunits, with oxidation of NADPH to NADP$^+$, slow inactivation[10,15,20], and high-frequency spiking going hand-in-hand[30].

Like the induction of sleep (Fig. 3b, c), these biophysical changes required the abrupt burst of ROS production caused by the high $^1O_2$ quantum yield[28] of miniSOG. No cell physiological changes—apart from a modest increase in input resistance—were seen after equally intense and prolonged irradiation of dFB neurons expressing membrane-bound GFP, whose chromophore is encased in a protein shell that prevents the close apposition of $O_2$ necessary for energy transfer (Extended Data Fig. 4a–e).

The coherent picture emerging from these within-cell analyses was mirrored in between-cell comparisons of neurons with chronically altered redox-sensing or redox-buffering capacity: the homozygous *Hyperkinetic* mutants carrying catalytically active or dead rescue transgenes that were our point of departure (Fig. 4f–j), or cells containing pro-oxidant[25,26] SOD1[A4V] or anti-oxidant[23] AOX (Fig. 4k–o). dFB neurons equipped with a functional Shaker β subunit expressed slowly inactivating A-type currents (Fig. 4i, j) that enabled high-frequency action potential trains (Fig. 4f, h). In flies forced to make do with the K289M mutant[15,20,21], which cannot convert NADPH to NADP^{+}, dFB neurons exhibited fast-inactivating $I_A$ (Fig. 4i, j), long interspike intervals (Fig. 4f, h), and shallow current-spike frequency functions (Fig. 4f, h) that can account for the insomnia of these animals (Fig. 1a, b). Profound shifts of Hyperkinetic's NADP^{+}:NADPH ratio in opposite directions must also underlie the divergent interspike interval distributions (Fig. 4k, m), current-spike frequency functions (Fig. 4k, m), and A-type inactivation kinetics of dFB neurons expressing SOD1[A4V] or AOX (Fig. 4n, o), which parallel large and opposite changes in daily sleep (Fig. 2c, d).

Because $K_V\beta$ subunits have extremely low cofactor exchange rates that limit catalysis [15,20], perhaps to a single hydride transfer[8], even a fleeting oxidant exposure will form a lasting biochemical memory. The Shaker–Hyperkinetic complex therefore unites three discrete functions in a single device: Its redox sensitivity allows it to monitor a key process relevant to sleep—the generation of oxidative by-products of mitochondrial electron transport. Its catalytic inefficiency allows the protein to compute and store the time integral of the resulting oxidative burden, as would be required if sleep's purpose were to protect against oxidative stress[14]. And its ability to set the spike frequency via conformational coupling to the channel's inactivation gate allows it to titrate the commensurate corrective action.

Before dFB neurons can discharge the accumulated sleep pressure, however, the inhibitory clamp imposed by Sandman must be released. This almost certainly involves the regulated endocytosis of the channel[5]. We suspect that Sandman's movements between intracellular storage vesicles and the cell surface are essential for the conversion of continuously varying sleep pressure into discrete sleep–wake states. Sharp transitions, not slow drift through twilight states, are of course the desired output of any sleep-control system. The exo-endocytic cycling of Sandman acts as an ON–OFF switch in the homeostatic feedback loop, allowing dFB neurons to alternate between 'fill' and 'discharge' modes[31]. In fill mode (that is, during waking), Sandman is present at the cell surface[5], action potentials are inhibited, and the Hyperkinetic pool fills with NADP^{+}. Sleep pressure builds but cannot be discharged until an unidentified signal arrives that causes the extraction of Sandman from the plasma membrane. At this point, the neurons switch to discharge mode, electrical activity resumes at the level dictated by the NADP^{+}:NADPH ratio of the Hyperkinetic pool, and the animal goes to sleep.

In order to dissipate the accumulated sleep pressure, the NADP^{+}:NADPH ratio must return to baseline during sleep. An elegant way to accomplish this reset would be to gate Hyperkinetic's enzymatic activity by voltage[8,20]. Cofactor release from the active site would be impeded in fill mode because the membrane potential of dFB neurons remains below the activation threshold of Shaker, but in discharge mode, the action potential-driven

rearrangements of the channel would open an escape path for $NADP^+$. Bidirectional coupling of a redox-modulated ion channel and a voltage-modulated oxidoreductase may thus be the accounting principle at the heart of the somnostat.

## Methods

### *Drosophila* strains and culture

Fly stocks were grown on media of sucrose, yeast, molasses, and agar under a 12 h light : 12h dark cycle at 25 °C. All studies were performed on randomly selected females aged 2–6 days post eclosion. Experimental flies were heterozygous for all transgenes and homozygous for either a wild-type or mutant (*Hk^1*) *Hyperkinetic* allele[32,33], as indicated. Driver lines *R23E10-GAL4*[34], *cry-GAL4*[35], *pdf-GAL4*[36], *OK107-GAL4*[37], and *GH146-GAL4*[38] were used to target dFB neurons, cryptochrome- or PDF-expressing clock neurons, Kenyon cells, or olfactory projection neurons, respectively. Effector transgenes encoded a fluorescent marker for visually guided patch-clamp recordings (*UAS-CD8::GFP*[39]); wild-type or mutant (*Hk^K289M*) *Hyperkinetic* rescue transgenes[21]; an optical integrator of ROS exposure in the mitochondrial matrix (*UAS-MitoTimer*[22]); the mitochondrial alternative oxidase AOX[24]; wild-type[40] and mutant[41] ($SOD1^{A4V}$) versions of human superoxide dismutase 1; catalase[42]; an N-myristoylated covalent hexamer[29] (myr-MS6T2) of the singlet oxygen generator miniSOG[28]; and RNAi constructs[43] for interference with the expression of *Hyperkinetic*, *Shaker*, *Shal*, or *cryptochrome* (101402KK, 104474KK, 103363KK, and 7238GD or 105172KK, respectively; Vienna *Drosophila* Resource Center).

### Sleep measurements

In standard sleep assays, females aged 3–5 d were individually inserted into 65-mm glass tubes, loaded into the Trikinetics *Drosophila* Activity Monitor system, and housed under 12 h light : 12h dark conditions. Periods of inactivity lasting at least 5 minutes were classified as sleep[44,45]. Immobile flies (< 2 beam breaks per 24 h) were excluded from the analysis. In sleep deprivation experiments, a spring-loaded platform stacked with Trikinetics monitors was slowly tilted by an electric motor, released, and allowed to snap back to its original position[46]. The mechanical cycles lasted 12 s and were repeated continuously.

Arousal thresholds in standard sleep assays were determined with the help of mechanical stimuli generated by vibration motors (Precision Microdrives, model 310-113) [47]. Stimuli were delivered once every hour, and the percentages of sleeping flies awakened within 5 minutes of each 5-s stimulation episode were quantified.

Sleep after light-induced ROS generation was measured at zeitgeber time 9.5 h. Female flies aged 3–5 d and expressing miniSOG in dFB neurons were individually inserted into 35-mm glass tubes and loaded into a custom-built array of light-tight chambers[31]. Each chamber was equipped with a high-power LED (Osram Opto Semiconductors LB W5SM-FZHX-35-0, 467 nm) running on an 80% duty cycle at 10 Hz and delivering 8 mW $cm^{-2}$ at the distal and 80 mW $cm^{-2}$ at the proximal end of the tube. In this intensity range, each miniSOG molecule in the central brain underwent an estimated 2–40 excitation cycles $s^{-1}$, based on the measured optical transmission of 7 fly heads at 467 nm (4.8 ± 0.3% (mean ±

s.e.m.), assumed to be isotropic) and a miniSOG absorption cross-section[28] of $5.0 \times 10^{-17}$ $cm^{-2}$.

The apparatus was operated in a temperature-controlled incubator (Sanyo MIR-154) at 25 °C. Excess heat from the high-power LEDs was removed by a water-cooling device incorporating liquid heat exchangers (Thermo Electric Devices LI102), a centrifugal pump (RS 702-6891), Peltier module (Adaptive ETC-128-10-05-E), and CPU cooler (Corsair CW-9060007-WW). For movement tracking, the chambers were continuously illuminated by low-power infrared (850 nm) LEDs from below and imaged from above at 25 frames $s^{-1}$ with a high-resolution CMOS camera (Thorlabs DCC1545M), using an 8 mm lens (Thorlabs MVL8M23) and a long-pass filter (Thorlabs, FEL800nm) to reject photostimulation light. A virtual instrument written in LabVIEW (National Instruments) extracted real-time position data from video images by subtracting the most recently acquired image from a temporally low-pass-filtered background[31]. Non-zero pixels in the difference image indicated that a movement had occurred, with the centroid of the largest cluster of non-zero pixels taken to represent the fly's new position. To eliminate noise, intensity and size thresholds were applied to pixel clusters in the difference image, and movements <2.5 mm (approximately one body length) were discarded. Periods of inactivity lasting at least 5 minutes were classified as sleep[44,45]. The flies were monitored for 10 min before the photooxidation of miniSOG, and subjects found asleep during that period were excluded from the analysis. Only individuals with a confirmed waking time >30 s were used to quantify waking movements, which were counted as distinct events if they were separated by >5 s of immobility.

## Functional imaging

Single-housed females were analysed 2–6 days post eclosion after 12 or 24 h of mechanical sleep deprivation[46], begun at zeitgeber times 0 h (daytime deprivation) or 12 h (night-time deprivation), and compared to age-matched controls at the end of sleep deprivation. After head-fixing the flies to a custom mount with eicosane (Sigma), cuticle, adipose tissue, and trachea were removed to create a small surgical window, and the brain was continuously superfused with extracellular solution equilibrated with 95% $O_2$–5% $CO_2$ and containing 103 mM NaCl, 3 mM KCl, 5 mM TES, 8 mM trehalose, 10 mM glucose, 7 mM sucrose, 26 mM $NaHCO_3$, 1 mM $NaH_2PO_4$, 1.5 mM $CaCl_2$, 4 mM $MgCl_2$, pH 7.3.

MitoTimer fluorescence was imaged *in vivo* by two-photon laser-scanning microscopy. Excitation light pulses with 140 fs duration and a centre wavelength of 910 nm (Chameleon Ultra II, Coherent) were intensity-modulated with the help of a Pockels cell (302RM, Conoptics) and focused by a 20×, 1.0 NA water immersion objective (W-Plan-Apochromat, Zeiss) on a Movable Objective Microscope (Sutter Instruments). Emitted photons were separated from excitation light by a series of dichromatic mirrors and dielectric and coloured glass filters, split into red and green channels (Semrock BrightLine FF01-571/72 and FF01-525/45, respectively), and detected by GaAsP photomultiplier tubes (H10770PA-40 SEL, Hamamatsu Photonics). Photocurrents were passed through high-speed amplifiers (HCA-4M-500K-C, Laser Components) and custom-designed integrator circuits to maximize the signal-to-noise ratio. The microscope was controlled through ScanImage

(Vidrio Technologies) via a PCI-6110 DAQ board (National Instruments). Images were acquired as z-stacks with an axial resolution of 1 μm.

Maximum-intensity projections of image stacks were analysed blind to sleep history, using a semi-automated script22 in MATLAB (The MathWorks). The algorithm rejected saturated or MitoTimer-negative pixels (fluorescence <1.5-fold above the mean of a manually defined background area) and calculated the average red-to-green ratio for the remaining image area.

## Electrophysiology

For whole-cell patch-clamp recordings *in vivo*, female flies aged 3–5 days post eclosion were prepared as for functional imaging, but the perineural sheath was also removed for electrode access. The somata of GFP-labeled dFB neurons were visually targeted with borosilicate glass electrodes (12–14 MΩ). The internal solution contained 140 mM potassium aspartate, 10 mM HEPES, 1 mM KCl, 4 mM MgATP, 0.5 mM $Na_3GTP$, 1 mM EGTA, pH 7.3. Signals were acquired with a Multiclamp 700B amplifier (Molecular Devices), filtered at 6–10 kHz, and digitised at 10–20 kHz using an ITC-18 data acquisition board (InstruTECH) controlled by the Nclamp/Neuromatic package. Data were analysed using Neuromatic software (www.neuromatic.thinkrandom.com) and custom procedures in Igor Pro (Wavemetrics).

For photostimulation of miniSOG during whole-cell recordings, a 455-nm LED (Thorlabs M455L3) was focused onto the head of the fly with a mounted f = 20.1 mm aspheric condenser lens (Thorlabs ACP2520-A) and controlled by a TTL-triggered dimmable constant-current LED driver (Thorlabs LEDD1B). The optical power at the sample was ~3.5 mW $cm^{-2}$.

Membrane resistances were calculated from linear fits of the steady-state voltage changes elicited by 1-s steps of hyperpolarizing currents (5-pA increments) from a pre-pulse potential of –60 ± 5 mV. Membrane time constants were estimated by fitting a single exponential to the voltage deflection caused by a hyperpolarizing 10 pA current step lasting 200 ms. Interspike intervals were determined from voltage responses to a standard series of depolarizing current steps (5 pA increments from 0 to 100 pA, 1 s duration). Spikes were detected by finding minima in the time derivative of the membrane potential trace. Interspike intervals at all levels of injected current were pooled for the calculation of frequency distributions.

Voltage-clamp experiments were performed in the presence of 1 μM tetrodotoxin (Tocris) and 200 μM cadmium to block sodium and calcium channels, respectively. Neurons were stepped from holding potentials of –110 or –30 mV to a test potential of +40 mV. When the cells were held at –110 mV, depolarization steps (1 s duration) elicited the full complement of potassium currents; when the cells were held at –30 mV, voltage-gated channels inactivated and the evoked potassium currents lacked the $I_A$ (A-type or fast outward) component48. Digital subtraction of the non-A-type component from the full complement of potassium currents gave an estimate of $I_A$. To determine the fast and slow inactivation time constants, double-exponential functions were fit to the decaying phase of currents elicited by 1-s depolarizing voltage pulses after digitally subtracting non-inactivating outward currents

(Extended Data Table 1). In cases where the fits of slow inactivation time constants were poorly constrained, only the fast inactivation time constants were included in the analysis.

## Statistics and reproducibility

Data were analysed in Prism 7 (GraphPad). Statistical detail, including test statistics, degrees of freedom, and exact $P$ values (to four significant digits) is reported in Supplementary Tables 1 and 2.

All null hypothesis tests were two-sided. Group means were compared by two-sided $t$-test or one-way or two-way ANOVA, using repeated measures designs or the Welch correction where indicated, followed by planned pairwise post-hoc analyses using Holm-Šídák's multiple comparisons test. Where the assumption of normality was violated (as indicated by Shapiro-Wilk test), group means were compared by two-sided Mann-Whitney test, two-sided Wilcoxon signed-rank test, or Kruskal-Wallis ANOVA; the latter was followed by Dunn's multiple comparisons test. $\chi^2$ or Fisher's exact tests were performed on contingency tables of categorical data, as noted. Interspike interval distributions were evaluated by two-sided Kolmogorov-Smirnov test. Figure legends give $P$ value ranges if multiple post-hoc tests were performed after ANOVA; the $P$ values of individual comparisons are found in Supplementary Tables 1 and 2.

The investigators were blind to group allocation in MitoTimer imaging experiments but not otherwise. Sample sizes in behavioural experiments (typically $n$=32 flies per genotype) were chosen to detect 2-h differences in daily sleep with a power of 0.9. All behavioural experiments were run at least three times, on different days and with different batches of flies. The figures show representative examples.
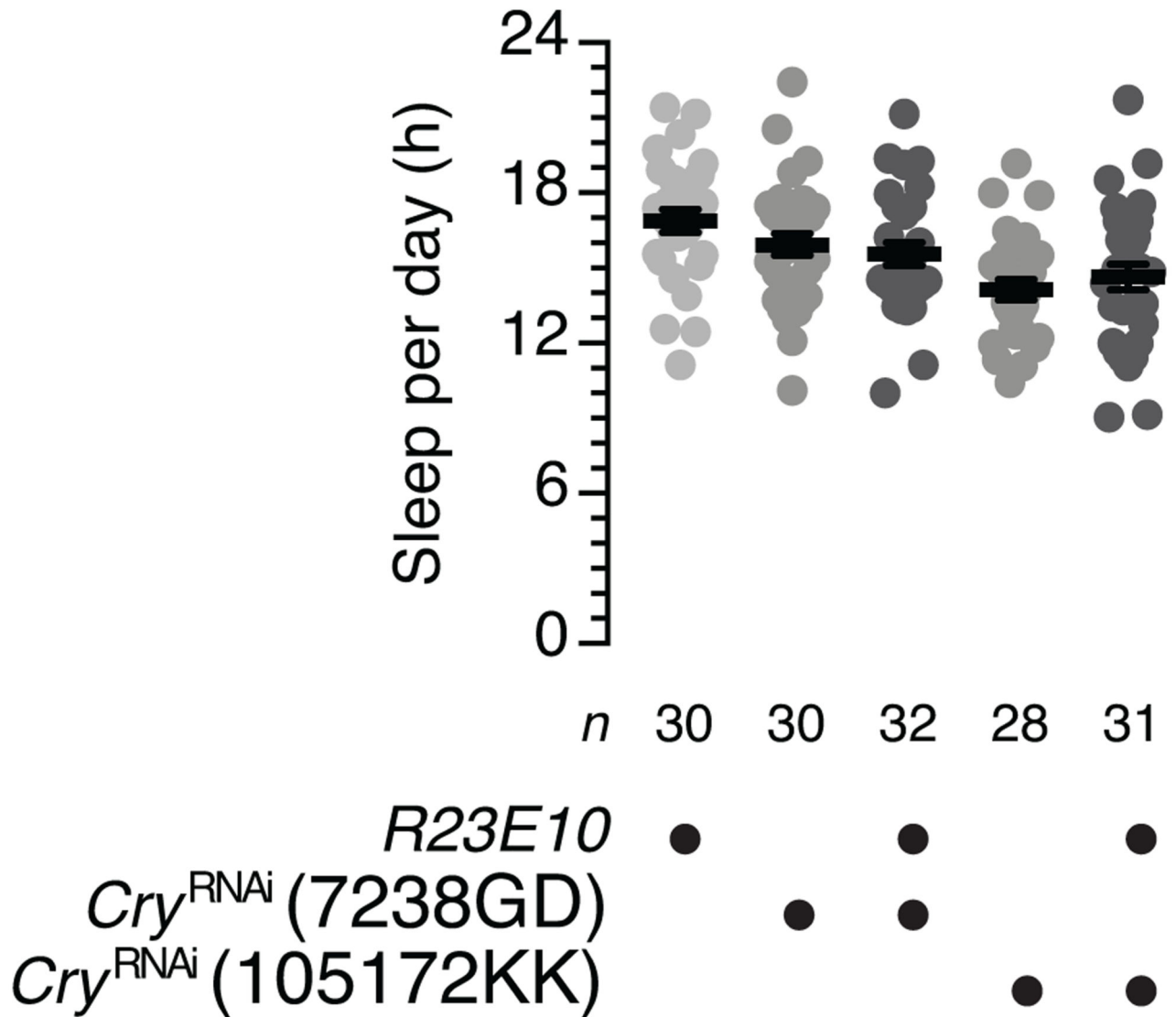
## Extended Data
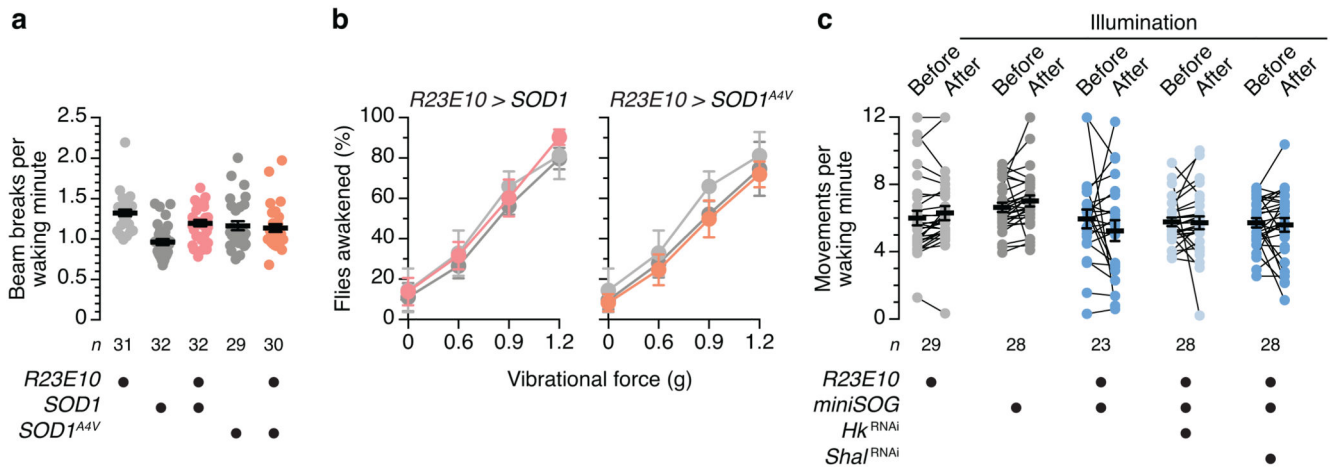
**Extended Data Figure 1. Chronic or acute dFB-restricted perturbations of redox chemistry have no impact on waking locomotor activity or arousability.**
**a**, Locomotor counts per waking minute of flies expressing *R23E10-GAL4*-driven SOD1 or pro-oxidant variant SOD1$^{A4V}$, in the Trikinetics *Drosophila* Activity Monitor system, do not differ from their respective parental controls (genotype effect: $P > 0.2612$, Kruskal-Wallis ANOVA with Dunn's post-hoc test). **b**, Arousability of flies expressing *R23E10-GAL4*-driven SOD1 (left) or pro-oxidant SOD1$^{A4V}$ (right) and parental controls (gray colours as in **a**) (genotype effects: $P > 0.2487$, vibrational force effects: $P < 0.0001$, vibrational force $\times$ genotype interactions: $P > 0.9857$, two-way ANOVA). Data are means $\pm$ s.e.m. of 6 trials per genotype ($n = 16$–32 flies each). **c**, Locomotor counts per waking minute of flies expressing *R23E10-GAL4*-driven miniSOG, with or without *RNAi* transgenes targeting $K_V$ channel subunits, and parental controls, in a custom video-tracking system31. Activity was monitored for 10 min before the photooxidation of miniSOG and then for a 30-min interval that included a 9-min exposure to blue light (genotype effect: $P = 0.0827$, illumination effect: $P = 0.8059$, illumination $\times$ genotype interaction: $P = 0.3086$, two-way repeated-measures ANOVA). Data are means $\pm$ s.e.m. *n*, number of flies (**a**, **c**) or trials (**b**). Statistical detail in Supplementary Table 2.
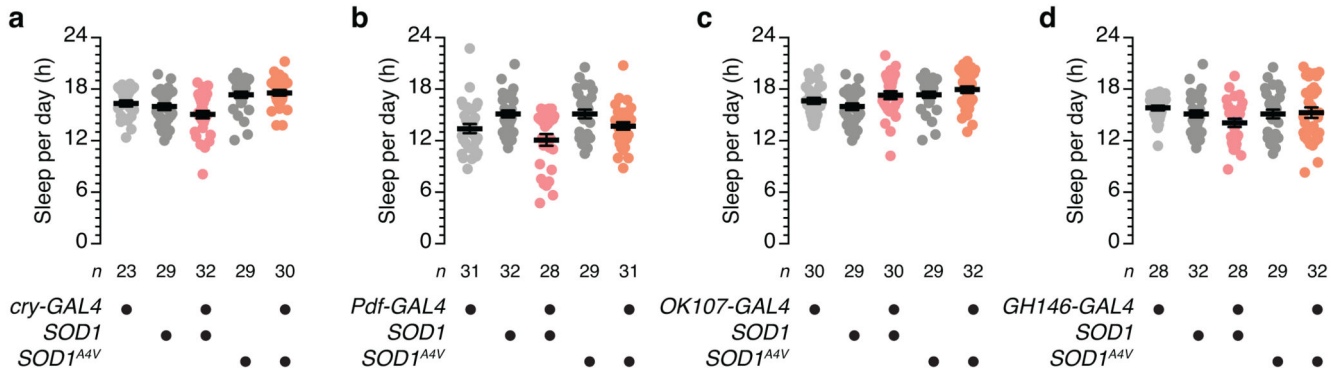
**Extended Data Figure 2. Chronic perturbations of redox chemistry in cryptochrome- or Pdf-expressing clock neurons, Kenyon cells, or olfactory projection neurons have no impact on sleep.**
**a**, Sleep in flies expressing *cry-GAL4*-driven SOD1 or SOD1[A4V] in clock neurons and parental controls. Kruskal-Wallis ANOVA with Dunn's post-hoc test failed to detect significant differences of experimental flies from both of their respective parental controls ($P$>0.1426). **b**, Sleep in flies expressing *Pdf-GAL4*-driven SOD1 or SOD1[A4V] in clock neurons and parental controls. Kruskal-Wallis ANOVA with Dunn's post-hoc test failed to detect significant differences of experimental flies from both of their respective parental controls ($P$>0.1732). **c**, Sleep in flies expressing *OK107-GAL4*-driven SOD1 or SOD1[A4V] in Kenyon cells and parental controls. One-way ANOVA with Holm-Šídák's post-hoc test failed to detect significant differences of experimental flies from both of their respective parental controls ($P$>0.0603). **d**, Sleep in flies expressing *GH146-GAL4*-driven SOD1 or SOD1[A4V] in olfactory projection neurons and parental controls. Kruskal-Wallis ANOVA with Dunn's post-hoc test failed to detect significant differences of experimental flies from both of their respective parental controls ($P$>0.6901). Data are means ± s.e.m. *n*, number of flies. Statistical detail in Supplementary Table 2.

**Extended Data Figure 3. Chronic dFB-restricted manipulations of cryptochrome have no impact on sleep.**
Sleep in flies expressing two different *R23E10-GAL4*-driven *cry*RNAi transgenes and parental controls. One-way ANOVA with Holm-Šídák's post-hoc test failed to detect significant differences of experimental flies from both of their respective parental controls ($P>0.1718$). Date are means ± s.e.m. *n*, number of flies. Statistical detail in Supplementary Table 2.
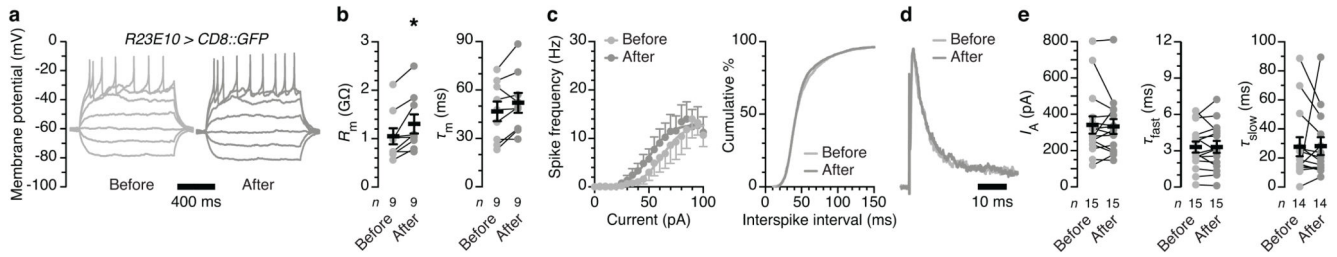
**Extended Data Figure 4. Blue illumination of miniSOG-negative dFB neurons has no impact on their electrical activity.**

**a**–**e**, dFB neurons expressing *R23E10-GAL4*-driven CD8::GFP, before and after a 9-min exposure to blue light. Example voltage responses to current steps (**a**, sample sizes in **b**): illumination increases the input resistance (**b**, $R_m$; $P$=0.0098, paired $t$-test) but not the membrane time constant (**b**, $\tau_m$; $P$=0.0723, paired $t$-test) and leaves unchanged the current-spike frequency function (**c**, left; current × genotype interaction: $P$=0.9982, two-way repeated-measures ANOVA) and interspike interval distribution (**c**, right; $P$=0.0947, Kolmogorov-Smirnov test). Example $I_A$ (normalized to peak) evoked by voltage steps to +40 mV (**d**, sample sizes in **e**): illumination leaves unchanged the $I_A$ amplitude (**e**; $P$=0.8040, Wilcoxon test) and both inactivation time constants (**e**, $\tau_{fast}$: $P$=0.6387, $\tau_{slow}$: $P$=0.2958, Wilcoxon tests). Asterisks indicate significant differences ($P$<0.05). Data are means ± s.e.m. *n*, number of cells. Statistical detail in Supplementary Table 2.

<div align="center">

**Extended Data Table 1**
**Parameters of $I_A$ inactivation.**

</div>

Inactivation time constants of $I_A$ evoked by voltage steps to +40 mV were obtained by fitting double-exponential functions to the decaying phase. $A_{fast}/(A_{fast}+A_{slow})$ represents the fraction of the fast component of the total A-current. Data are means ± s.e.m. *n*, number of cells. All dFB neurons expressed CD8::GFP in addition to the indicated transgenes.

## Supplementary Material

Refer to Web version on PubMed Central for supplementary material.

## Acknowledgments

## References

1. Rechtschaffen A. Current perspectives on the function of sleep. Perspect Biol Med. 1998; 41:359–390. [PubMed: 9604368]

2. Mignot E. Why we sleep: the temporal organization of recovery. PLoS Biol. 2008; 6:e106. [PubMed: 18447584]

3. Donlea JM, Thimgan MS, Suzuki Y, Gottschalk L, Shaw PJ. Inducing sleep by remote control facilitates memory consolidation in *Drosophila*. Science. 2011; 332:1571–1576. [PubMed: 21700877]

4. Donlea JM, Pimentel D, Miesenböck G. Neuronal machinery of sleep homeostasis in *Drosophila*. Neuron. 2014; 81:860–872. [PubMed: 24559676]

5. Pimentel D, et al. Operation of a homeostatic sleep switch. Nature. 2016; 536:333–337. [PubMed: 27487216]

6. Balaban RS, Nemoto S, Finkel T. Mitochondria, oxidants, and aging. Cell. 2005; 120:483–495. [PubMed: 15734681]

7. Murphy MP. How mitochondria produce reactive oxygen species. Biochem J. 2009; 417:1–13. [PubMed: 19061483]

8. Gulbis JM, Mann S, MacKinnon R. Structure of a voltage-dependent $K^+$ channel beta subunit. Cell. 1999; 97:943–952. [PubMed: 10399921]

9. Long SB, Campbell EB, MacKinnon R. Crystal structure of a mammalian voltage-dependent Shaker family $K^+$ channel. Science. 2005; 309:897–903. [PubMed: 16002581]

10. Chouinard SW, Wilson GF, Schlimgen AK, Ganetzky B. A potassium channel beta subunit related to the aldo-keto reductase superfamily is encoded by the *Drosophila* Hyperkinetic locus. Proc Natl Acad Sci USA. 1995; 92:6763–6767. [PubMed: 7542775]

11. Bushey D, Huber R, Tononi G, Cirelli C. *Drosophila* Hyperkinetic mutants have reduced sleep and impaired memory. J Neurosci. 2007; 27:5384–5393. [PubMed: 17507560]

12. Orr WC, Sohal RS. Extension of life-span by overexpression of superoxide dismutase and catalase in *Drosophila* melanogaster. Science. 1994; 263:1128–1130. [PubMed: 8108730]

13. Cirelli C, et al. Reduced sleep in *Drosophila* Shaker mutants. Nature. 2005; 434:1087–1092. [PubMed: 15858564]

14. Hill VM, et al. A bidirectional relationship between sleep and oxidative stress in *Drosophila*. PLoS Biol. 2018; 16:e2005206. [PubMed: 30001323]

15. Weng J, Cao Y, Moss N, Zhou M. Modulation of voltage-dependent Shaker family potassium channels by an aldo-keto reductase. J Biol Chem. 2006; 281:15194–15200. [PubMed: 16569641]

16. Tipparaju SM, Barski OA, Srivastava S, Bhatnagar A. Catalytic mechanism and substrate specificity of the beta-subunit of the voltage-gated potassium channel. Biochemistry. 2008; 47:8840–8854. [PubMed: 18672894]

17. Sherin JE, Shiromani PJ, McCarley RW, Saper CB. Activation of ventrolateral preoptic neurons during sleep. Science. 1996; 271:216–219. [PubMed: 8539624]

18. Connor JA, Stevens CF. Prediction of repetitive firing behaviour from voltage clamp data on an isolated neurone soma. J Physiol (Lond). 1971; 213:31–53. [PubMed: 5575343]

19. McCormack T, McCormack K. Shaker $K^+$ channel beta subunits belong to an NAD(P)H-dependent oxidoreductase superfamily. Cell. 1994; 79:1133–1135. [PubMed: 8001150]

20. Pan Y, Weng J, Cao Y, Bhosle RC, Zhou M. Functional coupling between the Kv1.1 channel and aldoketoreductase Kvbeta1. J Biol Chem. 2008; 283:8634–8642. [PubMed: 18222921]

21. Fogle KJ, et al. CRYPTOCHROME-mediated phototransduction by modulation of the potassium ion channel β-subunit redox sensor. Proc Natl Acad Sci USA. 2015; 112:2245–2250. [PubMed: 25646452]

22. Laker RC, et al. A novel MitoTimer reporter gene for mitochondrial content, structure, stress, and damage in vivo. J Biol Chem. 2014; 289:12005–12015. [PubMed: 24644293]

23. Maxwell DP, Wang Y, McIntosh L. The alternative oxidase lowers mitochondrial reactive oxygen production in plant cells. Proc Natl Acad Sci USA. 1999; 96:8271–8276. [PubMed: 10393984]

24. Fernandez-Ayala DJM, et al. Expression of the Ciona intestinalis alternative oxidase (AOX) in *Drosophila* complements defects in mitochondrial oxidative phosphorylation. Cell Metab. 2009; 9:449–460. [PubMed: 19416715]

25. Wiedau-Pazos M, et al. Altered reactivity of superoxide dismutase in familial amyotrophic lateral sclerosis. Science. 1996; 271:515–518. [PubMed: 8560268]

26. Yim MB, et al. A gain-of-function of an amyotrophic lateral sclerosis-associated Cu,Zn-superoxide dismutase mutant: An enhancement of free radical formation due to a decrease in $K_m$ for hydrogen peroxide. Proc Natl Acad Sci USA. 1996; 93:5709–5714. [PubMed: 8650157]

27. Artiushin G, Sehgal A. The *Drosophila* circuitry of sleep-wake regulation. Curr Opin Neurobiol. 2017; 44:243–250. [PubMed: 28366532]

28. Shu X, et al. A genetically encoded tag for correlated light and electron microscopy of intact cells, tissues, and organisms. PLoS Biol. 2011; 9:e1001041. [PubMed: 21483721]

29. Ng J, et al. Genetically targeted 3D visualisation of *Drosophila* neurons under electron microscopy and X-ray microscopy using miniSOG. Sci Rep. 2016; 6

30. Yao WD, Wu CF. Auxiliary Hyperkinetic beta subunit of $K^+$ channels: regulation of firing properties and $K^+$ currents in *Drosophila* neurons. J Neurophysiol. 1999; 81:2472–2484. [PubMed: 10322082]

31. Donlea JM, et al. Recurrent circuitry for balancing sleep need and sleep. Neuron. 2018; 97:378–389.e4. [PubMed: 29307711]

32. Kaplan WD, Trout WE. The behavior of four neurological mutants of *Drosophila*. Genetics. 1969; 61:399–409. [PubMed: 5807804]

33. Stern M, Ganetzky B. Altered synaptic transmission in *Drosophila hyperkinetic* mutants. J Neurogenet. 1989; 5:215–228. [PubMed: 2553904]

34. Jenett A, et al. A GAL4-driver line resource for *Drosophila* neurobiology. Cell Rep. 2012; 2:991–1001. [PubMed: 23063364]

35. Kaneko M, Park JH, Cheng Y, Hardin PE, Hall JC. Disruption of synaptic transmission or clock-gene-product oscillations in circadian pacemaker cells of *Drosophila* cause abnormal behavioral rhythms. J Neurobiol. 2000; 43:207–233. [PubMed: 10842235]

36. Renn SCP, Park JH, Rosbash M, Hall JC, Taghert PH. A pdf neuropeptide gene mutation and ablation of PDF neurons each cause severe abnormalities of behavioral circadian rhythms in *Drosophila*. Cell. 1999; 99:791–802. [PubMed: 10619432]

37. Tanaka NK, Tanimoto H, Ito K. Neuronal assemblies of the *Drosophila* mushroom body. J Comp Neurol. 2008; 508:711–755. [PubMed: 18395827]

38. Stocker RF, Heimbeck G, Gendre N, de Belle JS. Neuroblast ablation in *Drosophila P[GAL4]* lines reveals origins of olfactory interneurons. J Neurobiol. 1997; 32:443–456. [PubMed: 9110257]

39. Lee T, Luo L. Mosaic analysis with a repressible cell marker for studies of gene function in neuronal morphogenesis. Neuron. 1999; 22:451–461. [PubMed: 10197526]

40. Parkes TL, et al. Extension of *Drosophila* lifespan by overexpression of human SOD1 in motorneurons. Nat Genet. 1998; 19:171–174. [PubMed: 9620775]

41. Watson MR, Lagow RD, Xu K, Zhang B, Bonini NM. A *Drosophila* model for amyotrophic lateral sclerosis reveals motor neuron damage by human SOD1. J Biol Chem. 2008; 283:24972–24981. [PubMed: 18596033]

42. Anderson PR, Kirby K, Hilliker AJ, Phillips JP. RNAi-mediated suppression of the mitochondrial iron chaperone, frataxin, in *Drosophila*. Hum Mol Genet. 2005; 14:3397–3405. [PubMed: 16203742]

43. Dietzl G, et al. A genome-wide transgenic RNAi library for conditional gene inactivation in *Drosophila*. Nature. 2007; 448:151–156. [PubMed: 17625558]

44. Shaw PJ, Cirelli C, Greenspan RJ, Tononi G. Correlates of sleep and waking in *Drosophila melanogaster*. Science. 2000; 287:1834–1837. [PubMed: 10710313]

45. Hendricks JC, et al. Rest in *Drosophila* is a sleep-like state. Neuron. 2000; 25:129–138. [PubMed: 10707978]

46. Shaw PJ, Tononi G, Greenspan RJ, Robinson DF. Stress response genes protect against lethal effects of sleep deprivation in *Drosophila*. Nature. 2002; 417:287–291. [PubMed: 12015603]

47. van Alphen B, Yap MHW, Kirszenblat L, Kottler B, van Swinderen B. A dynamic deep sleep stage in *Drosophila*. J Neurosci. 2013; 33:6917–6927. [PubMed: 23595750]

48. Connor JA, Stevens CF. Voltage clamp studies of a transient outward membrane current in gastropod neural somata. J Physiol (Lond). 1971; 213:21–30. [PubMed: 5575340]
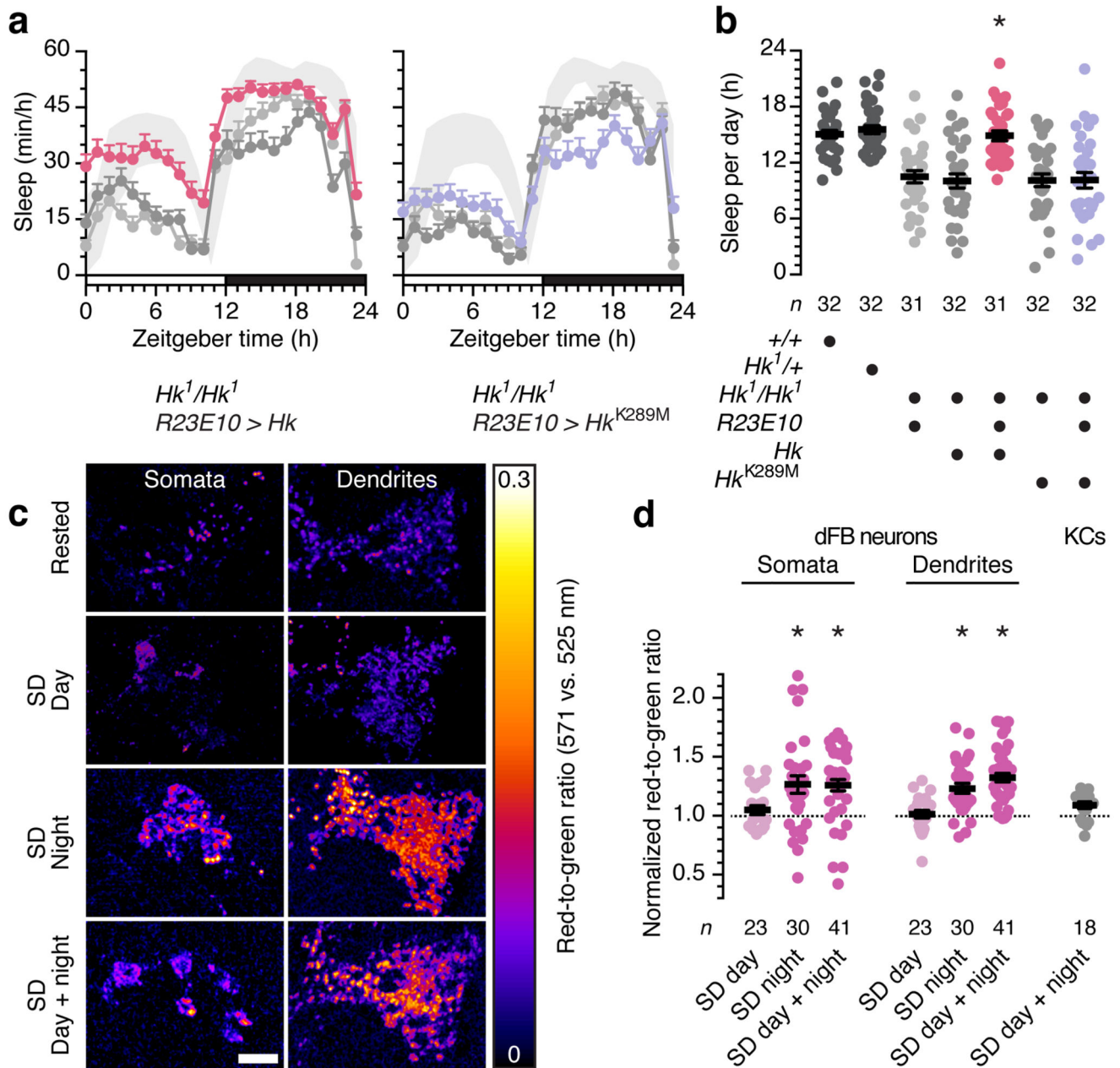
**Figure 1. Hyperkinetic senses redox changes linked to sleep history.**

**a**, *R23E10-GAL4*-driven expression of Hk (left), but not of Hk$^{K289M}$ (right), in a homozygous *Hk$^1$* mutant background restores wild-type sleep (shaded bands: 95% confidence intervals) relative to parental controls (gray colours and sample sizes as in **b**). Two-way repeated-measures ANOVA with Holm-Šídák's post-hoc test detected significant differences from both parental controls (*P*<0.0001) but not from wild-type (*P*=0.8599) in flies expressing Hk, and a significant difference from wild-type (*P*<0.0001) but not from either parental control (*P*>0.9741) in flies expressing Hk$^{K289M}$. **b**, Sleep in homozygous *Hk$^1$* mutants expressing *R23E10-GAL4*-driven *Hk* rescue transgenes and parental, wild-type, and

heterozygous controls. One-way ANOVA with Holm-Šídák's post-hoc test detected significant differences from both parental controls ($P<0.0001$) but not from wild-type ($P=0.9763$) in flies expressing Hk, and a significant difference from wild-type ($P<0.0001$) but not from either parental control ($P>0.9704$) in flies expressing Hk[K289M]. **c**, Example maximum intensity projections of the somata and dendritic arbors of dFB neurons expressing MitoTimer under *R23E10-GAL4* control, in rested and sleep-deprived (SD) flies (sample sizes in **d**). The red-to-green emission ratio is pseudocoloured according to the key on the right. Scale bar, 10 μm. **d**, Sleep deprivation during the night (SD effect: $P<0.0001$, Kruskal-Wallis ANOVA), but not during the day ($P>0.6416$, Mann-Whitney test), increases MitoTimer's red-to-green ratio in somata and dendrites of dFB neurons but not in Kenyon cells (KCs) ($P=0.1328$, *t*-test). Fluorescence ratios are normalized to those of unperturbed controls at the end of sleep deprivation ($n=22$ and 62 dFB controls for daytime and night-time deprivation; $n=20$ KC controls). Asterisks indicate significant differences ($P<0.05$) from both parental controls (**b**) or rested conditions (**d**) in pairwise post-hoc comparisons. Data are means ± s.e.m. *n*, number of flies. Statistical detail in Supplementary Table 1.
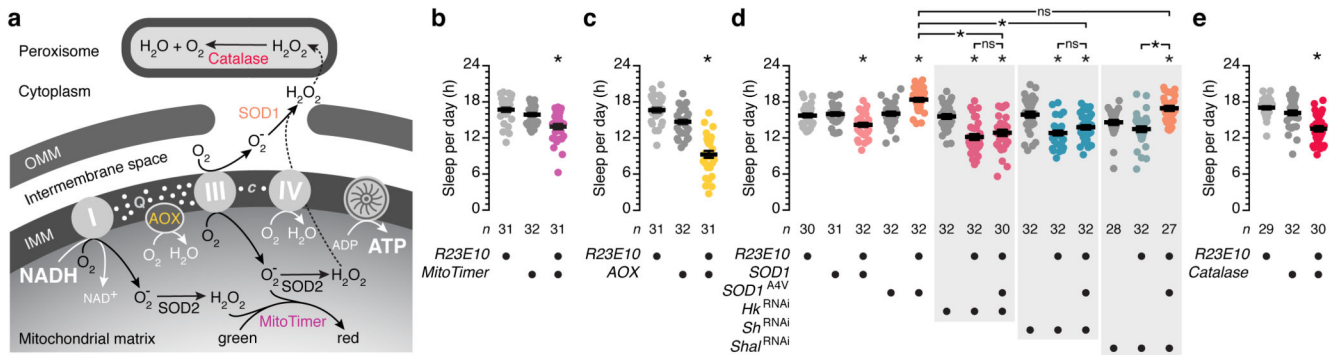
**Figure 2. dFB-restricted perturbations of redox chemistry alter sleep.**
**a**, Ubiquinone (Q) and cytochrome $c$ ($c$) ferry electrons (white dots) between the proton-pumping complexes I, III, and IV. When more electrons enter the transport chain than can be used to fuel ATP synthesis, a backlog accumulates in the Q pool. These electrons react directly with $O_2$, releasing $O_2^-$ into the matrix and the space between the inner and outer mitochondrial membranes (IMM and OMM). Superoxide dismutases (SOD2 in the matrix, SOD1 in the intermembrane space and cytoplasm) convert $O_2^-$ to membrane-permeant $H_2O_2$; catalase decomposes $H_2O_2$. AOX uses surplus Q electrons to reduce $O_2$ to water. Coloured components were manipulated in **b**–**e**. **b**, Sleep in flies expressing *R23E10-GAL4*-driven MitoTimer and parental controls (genotype effect: $P=0.0007$, one-way ANOVA). **c**, Sleep in flies expressing *R23E10-GAL4*-driven AOX and parental controls (genotype effect: $P<0.0001$, one-way ANOVA). **d**, Sleep in flies expressing *R23E10-GAL4*-driven SOD1 or pro-oxidant SOD1$^{A4V}$, with or without *RNAi* transgenes targeting $K_V$ channel subunits, and parental controls (genotype effect: $P<0.0001$, one-way ANOVA). **e**, Sleep in flies expressing *R23E10-GAL4*-driven catalase and parental controls (genotype effect: $P<0.0001$, one-way ANOVA). Asterisks indicate significant differences ($P<0.05$) from both parental controls or in relevant pairwise post-hoc comparisons (brackets). Data are means ± s.e.m. *n*, number of flies. Statistical detail in Supplementary Table 1.
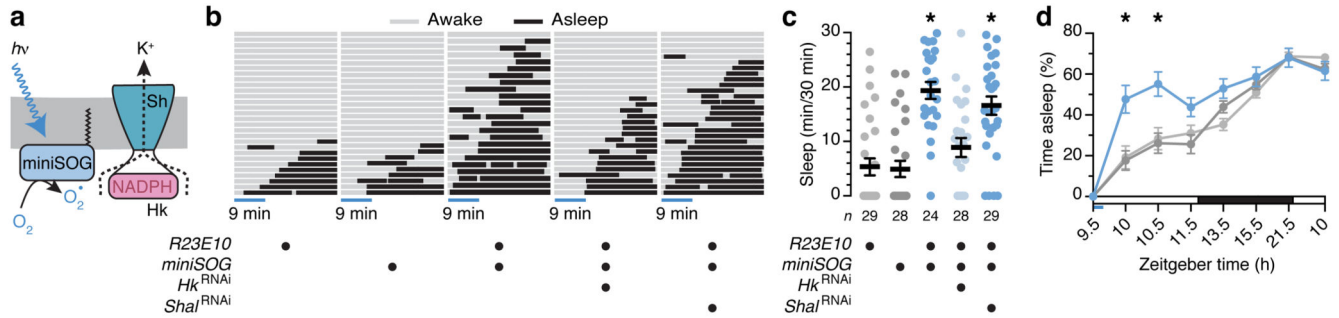
**Figure 3. Optogenetically controlled ROS production in dFB neurons induces sleep.**
**a**, N-myristoylated miniSOG near the Hyperkinetic (Hk) gondola underneath Shaker (Sh). **b**, Periods of wake (gray) and sleep (black) during and after an initial 9-min exposure to blue light, in flies expressing *R23E10-GAL4*-driven miniSOG, with or without *RNAi* transgenes targeting $K_V$ channel subunits, and parental controls. Each row depicts one individual; all individuals were awake at the onset of illumination. The fraction of experimental flies falling asleep differed from both parental controls ($P<0.0001$) and from flies coexpressing $Hk^{RNAi}$ ($P=0.0030$) but not $Shal^{RNAi}$ ($P=0.3622$, Fisher's exact test throughout, sample sizes in **c**). **c**, Sleep in flies expressing *R23E10-GAL4*-driven miniSOG, with or without *RNAi* transgenes targeting $K_V$ channel subunits, and parental controls (genotype effect: $P<0.0001$, Kruskal-Wallis ANOVA). **d**, Cumulative sleep percentages after a 9-min exposure to blue light at zeitgeber time 9.5 h, in flies expressing *R23E10-GAL4*-driven miniSOG ($n=19$) and parental controls ($n=25$ each, gray colours as in **c**) (time × genotype interaction: $P<0.0001$, two-way repeated-measures ANOVA). Asterisks indicate significant differences ($P<0.05$) from both parental controls or in relevant pairwise post-hoc comparisons. Data are means ± s.e.m. *n*, number of flies. Statistical detail in Supplementary Table 1.
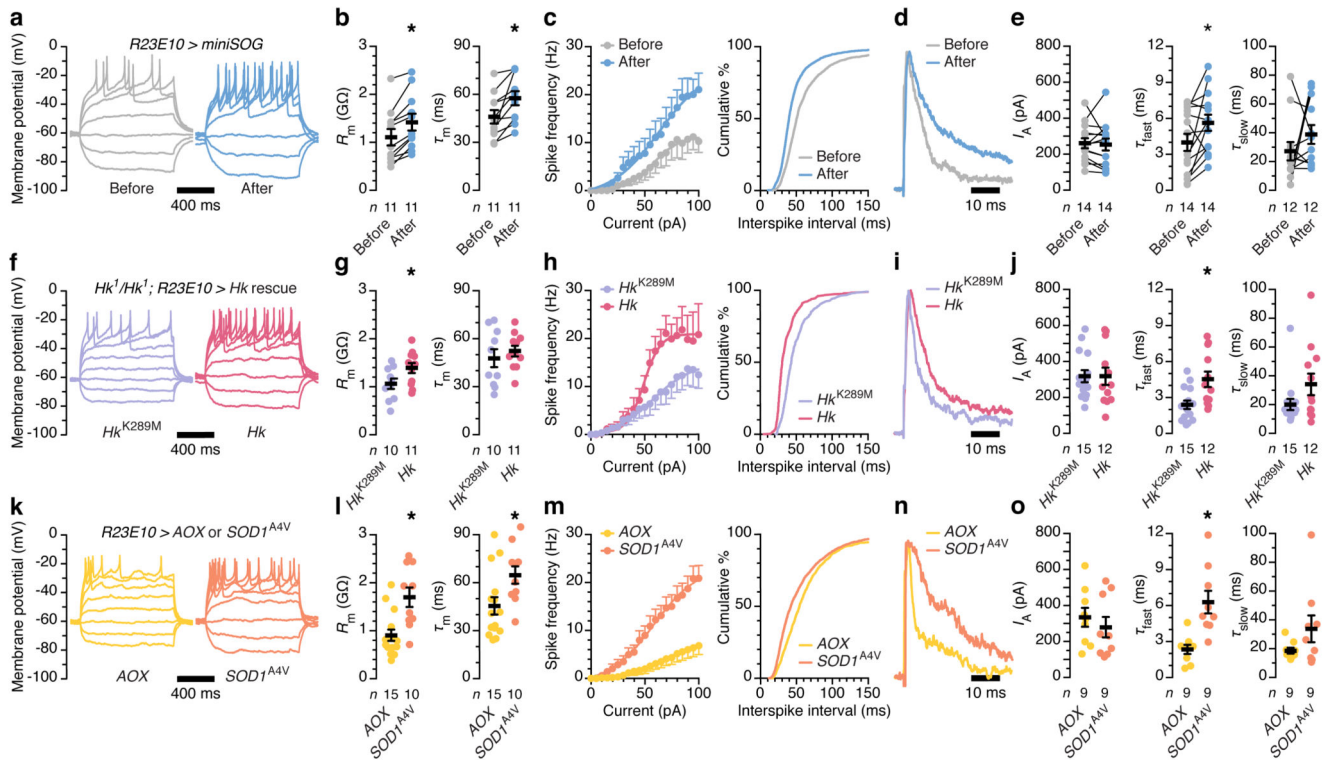
**Figure 4. Changes in redox chemistry alter the spiking activity of dFB neurons via $I_A$.**
**a–e**, dFB neurons expressing *R23E10-GAL4*-driven miniSOG and CD8::GFP, before and after a 9-min exposure to blue light. Example voltage responses to current steps (**a**, sample sizes in **b**): illumination increases the input resistance (**b**, $R_m$; $P<0.0001$, paired *t*-test) and membrane time constant (**b**, $\tau_m$; $P=0.0041$, paired *t*-test), steepens the current-spike frequency function (**c**, left; current × genotype interaction: $P=0.0014$, two-way repeated-measures ANOVA), and shifts the interspike interval distribution toward shorter values (**c**, right; $P<0.0001$, Kolmogorov-Smirnov test). Example $I_A$ (normalized to peak) evoked by voltage steps to +40 mV (**d**, sample sizes in **e**): illumination leaves the $I_A$ amplitude unchanged (**e**; $P=0.7295$, paired *t*-test) and increases the fast (**e**, $\tau_{fast}$; $P=0.0245$, Wilcoxon test) but not the slow inactivation time constant (**e**, $\tau_{slow}$; $P=0.3804$, Wilcoxon test). **f–j**, dFB neurons expressing *R23E10-GAL4*-driven $Hk^{K289M}$ or *Hk* rescue transgenes in a homozygous $Hk^1$ mutant background. Example voltage responses to current steps (**f**, sample sizes in **g**): catalytically competent Hk increases the input resistance (**g**, $R_m$; $P=0.0467$, *t*-test) but not the membrane time constant (**g**, $\tau_m$; $P=0.4962$, *t*-test), steepens the current-spike frequency function (**h**, left; current × genotype interaction: $P<0.0001$, two-way repeated-measures ANOVA), and shifts the interspike interval distribution toward shorter values (**h**, right; $P<0.0001$, Kolmogorov-Smirnov test). Example $I_A$ (normalized to peak) evoked by voltage steps to +40 mV (**i**, sample sizes in **j**): catalytically competent Hk leaves the $I_A$ amplitude unchanged (**j**; $P=0.9827$, *t*-test) and increases the fast (**j**, $\tau_{fast}$; $P=0.0061$, *t*-test) but not the slow inactivation time constant (**j**, $\tau_{slow}$; $P=0.1257$, Mann-Whitney test). **k–o**, dFB neurons expressing *R23E10-GAL4*-driven AOX or SOD1$^{A4V}$. Example voltage responses to current steps (**k**, sample sizes in **l**): pro-oxidant SOD1$^{A4V}$ increases the input

resistance (**l**, $R_m$; $P$=0.0023, Mann-Whitney test) and membrane time constant (**l**, $\tau_m$; $P$=0.0166, Mann-Whitney test), steepens the current-spike frequency function (**m**, left; current × genotype interaction: $P$<0.0001, two-way repeated-measures ANOVA), and shifts the interspike interval distribution toward shorter values (**m**, right; $P$<0.0001, Kolmogorov-Smirnov test). Example $I_A$ (normalized to peak) evoked by voltage steps to +40 mV (**n**, sample sizes in **o**): pro-oxidant SOD1$^{A4V}$ leaves the $I_A$ amplitude unchanged (**o**; $P$=0.4892, $t$-test) and increases the fast (**o**, $\tau_{fast}$; $P$=0.0027, $t$-test) but not the slow inactivation time constant (**o**, $\tau_{slow}$; $P$=0.3401, Mann-Whitney test). Asterisks indicate significant differences ($P$<0.05). Data are means ± s.e.m. *n*, number of cells. Statistical detail in Supplementary Table 1.